Chapter 4
Fundamentals of Laser-Material Interaction and Application to Multiscale Surface Modification

Matthew S. Brown and Craig B. Arnold

Abstract Lasers provide the ability to accurately deliver large amounts of energy into confined regions of a material in order to achieve a desired response. For opaque materials, this energy is absorbed near the surface, modifying surface chemistry, crystal structure, and/or multiscale morphology without altering the bulk. This chapter covers a brief introduction to the fundamental principles governing laser propagation and absorption as well as the resulting material responses. We then highlight two case studies of improving efficiency in photovoltaic and optoelectronic devices as well as optimizing cell-surface interactions in biological interfaces.

4.1 Introduction

Modification of surface properties over multiple length scales plays an important role in optimizing a material's performance for a given application. For instance, the cosmetic appearance of a surface and its absorption properties can be controlled by altering its texture [1, 2] and presence of chemical impurities in the surface [3]. A material's susceptibility to wear and surface damage can be reduced by altering its surface chemistry, morphology, and crystal structure [4]. Also, one can consider the frictional, adhesive, and wetting forces acting at a material interface as being strongly influenced by the size and shape of the micro and nanoscale features present [5]. As such, multiscale surface modifications are a critical factor in the development of new material structures and in engineering the detailed interactions that occur at surfaces and interfaces.

From the earliest work with pulsed ruby lasers, it has been understood that the unique interaction of laser light with a material can lead to permanent changes in the material's properties not easily achievable through other means. Laser irradiation

M.S. Brown and C.B. Arnold (✉)
Department of Mechanical and Aerospace Engineering, Princeton Institute for Science and Technology of Materials, Princeton University, Princeton, NJ 08544, USA
e-mail: msbrown@princeton.edu; cbarnold@princeton.edu

K. Sugioka et al. (eds.), *Laser Precision Microfabrication*,
Springer Series in Materials Science 135, DOI 10.1007/978-3-642-10523-4_4,

has been shown to induce changes to the local chemistry, the local crystal structure, and the local morphology, all of which affect how the material behaves in a given application. A number of fine books and review articles have been written on this subject [6–9]. The main issue here is the ability to precisely deposit a large amount of energy into a material over a short time scale and in a spatially confined region near the surface. This allows control of local surface properties relative to the bulk and relative to other regions on the surface. But perhaps more importantly, the effect of this incident energy, the interaction time scale, and other laser parameters can lead to material responses and changes that span multiple length scales, from the atomic to the macroscale.

Clearly, a complete treatment of all laser surface modifications and applications is beyond the scope of a single book chapter, so we will primarily focus on two specific case studies in which new applications are actively being developed. Before delving into these case studies, we start with a short review of the underlying principles and equations governing the absorption of laser light and the transport of heat inside the material. We discuss the fundamental material responses that can occur as well as some of the established applications of laser surface modification. We then turn to the first case study where we examine the multiscale morphological and chemical changes to the surfaces of laser irradiated metals and semiconductors, which allow optimized optical properties for such emerging applications as high efficiency solar cells, security, or microfluidics. In the second case study, we discuss how laser processing can be used to produce multiscale changes to the surface morphology and chemistry of biomaterials to enhance the adhesion of proteins and cells for applications such as biomedical implants and lab-on-a-chip type sensors.

4.2 Fundamentals of Laser Surface Processing

One of the major advantages of the laser as a tool for material processing is the ability to precisely control where in the material and at what rate energy is deposited. This control is exercised through the proper selection of laser processing parameters to achieve the desired material modification. In this section, we discuss the principles and equations that describe the propagation and absorption of laser energy and heat flow (also see Chaps. 2 and 8).

4.2.1 Light Propagation in Materials

Confinement of deposited energy to desired regions on a material's surface can be achieved by controlling the laser's spatial intensity profile. The predominant methods for control include beam steering by fixed or galvanometric scanning mirrors, beam focusing through telescoping or converging optics, and beam shaping with homogenizers [10], amplitude masks, refractive elements [11], and diffractive optical

elements (DOE) [12] (see Chaps. 3 and 10). However, one can also use more advanced optical devices such as spatial light modulators [13], deformable mirrors [14], and tunable acoustic gradient index (TAG) lenses [15] allowing real-time modulation of the beam's intensity profile on the surface (see Chaps. 1 and 3). There has been extensive work in the area of beam shaping with a number of articles and books [16, 17] as well as a chapter in this book devoted to the subject (Chap. 5).

When light strikes the surface of a material, a portion will be reflected from the interface due to the discontinuity in the real index of refraction and the rest will be transmitted into the material. The fraction of the incident power that is reflected from the surface R depends on the polarization and angle of incidence θ_i of the light as well as the index of refraction of the atmosphere n_1 and the material n_2. The reflection coefficients for the s-polarized and p-polarized components of the light can be calculated from the well known Fresnel equations [18]:

$$R_s = \left[\frac{E_r}{E_i}\right]^2 = \left[\frac{n_1 \cos(\theta_i) - n_2 \cos(\theta_t)}{n_1 \cos(\theta_i) + n_2 \cos(\theta_t)}\right]^2 \tag{4.1}$$

$$R_p = \left[\frac{E_r}{E_i}\right]^2 = \left[\frac{n_1 \cos(\theta_t) - n_2 \cos(\theta_i)}{n_1 \cos(\theta_t) + n_2 \cos(\theta_i)}\right]^2 \tag{4.2}$$

and are related to the transmission coefficients through $T_s = 1 - R_s$ and $T_p = 1 - R_p$. For the case of normally incident light on a flat surface, the above equations reduce to the more familiar form:

$$R = R_s = R_p = \left(\frac{n_1 - n_2}{n_1 + n_2}\right)^2 \tag{4.3}$$

The reflectivity of a given material will depend on the frequency of the light source through the dispersion relation of its index of refraction. For instance in the case of normal incidence, values for reflectivity of metals in the near UV and visible spectral range are typically between 0.4 and 0.95, and between 0.9 and 0.99 for the IR [7]. In addition, the reflectivity of a surface will depend on the temperature of the material through changes in the permittivity, band structure, plasma oscillations, or material phase [19]. For instance, upon melting, the reflectivity of silicon increases by a factor of about 2 [20], while that of a metal such as Ni changes by only a few percent [21]. In the case of small scale or structured materials, additional optical resonances are possible, such as surface and bulk plasmons and polaritons, which can lead to enhanced absorption or reflection due to the details of the photon–electron interactions [22].

Once inside the material, absorption causes the intensity of the light to decay with depth at a rate determined by the material's absorption coefficient α. In general, α is a function of wavelength and temperature, but for constant α, intensity I decays exponentially with depth z according to the Beer–Lambert law,

$$I(z) = I_0 \mathrm{e}^{-\alpha z} \tag{4.4}$$

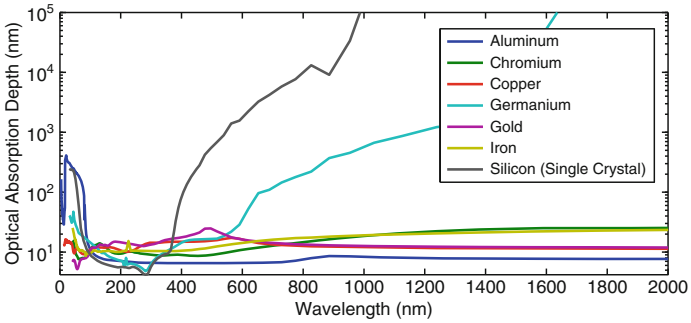

Fig. 4.1 Optical absorption depths for several materials over a range of wavelengths [23]

where I_0 is the intensity just inside the surface after considering reflection loss. The magnitude of the gradient of intensity yields the volumetric energy deposition rate $\alpha I_0 \mathrm{e}^{-\alpha z}$.

It is convenient to define the optical penetration or absorption depth, $\delta = 1/\alpha$, which is the depth at which the intensity of the transmitted light drops to $1/e$ of its initial value at the interface. Figure 4.1 shows optical absorption depths as a function of wavelength for a variety of metals and semiconductors. The important thing to note from Fig. 4.1 is that the absorption depths are short relative to bulk material dimensions. For instance, in the case of most metals undergoing UV illumination, the absorption depth is on the order of 10 nm. Although the interpretation of absorption depth was developed for a plane wave, the fact that energy absorption is approximately confined within the absorption depth still holds for more general beam profiles. Therefore, choosing wavelength with short absorption depths can allow local modification of surface properties without altering the bulk of the material.

The above treatments considered only linear optical phenomena; however, this is not necessarily the case in all materials, nor for all incident laser conditions. Some materials such as glasses exhibit strong non-linearities in their index of refraction [24], which can lead to a number of interesting effects such as self-focusing, defocusing, or soliton propagation [25]. When dealing with CW or nanosecond duration laser pulses, it is typically assumed that most of the absorption is due to single photon interactions. However, for picosecond (ps) and femtosecond (fs) lasers, the extremely high instantaneous intensity enables phenomena such as optical breakdown and multiphoton absorption which can significantly decrease absorption depths [26]. Effects such as these will change the fundamental material interactions and are discussed in more detail in Chaps. 8 and 9.

4.2.2 Energy Absorption Mechanisms

The absorption coefficient, which can be derived from the material's dielectric function and conductivity, determines the absorption of light as a function of depth.

However, the specific mechanisms by which the absorption occurs will depend on the type of material. In general, photons will couple into the available electronic or vibrational states in the material depending on the photon energy. In insulators and semiconductors, the absorption of laser light predominantly occurs through resonant excitations such as transitions of valence band electrons to the conduction band (interband transitions) or within bands (intersubband transitions) [7]. These excited electronic states can then transfer energy to lattice phonons. Photons with energy below the material's band gap will not be absorbed (unless there are other impurity or defect states to couple to or if there is multiphoton absorption). Such energies typically correspond to light frequencies below vacuum ultraviolet for insulators and below the visible to infrared spectrum for semiconductors. However, resonant coupling to high-frequency optical phonons in the near-infrared region is possible in some cases [27].

In metals, optical absorption is dominated by the free electrons through such mechanisms as inverse bremsstrahlung [28]. Energy is subsequently transferred to lattice phonons by collisions. An important parameter relating the electron density of a metal N_e to its optical properties is the plasma frequency $\omega_p = \sqrt{N_e e^2/m_e \varepsilon_0}$, where m_e is the mass of an electron and ε_0 the permittivity of free space. Reflectivity and absorptance for light frequencies below the plasma frequency are high because electrons in the metal screen the electric field of the light. However, above the plasma frequency, reflectivity and absorptance drop off drastically because the electrons cannot respond fast enough to screen it [29]. Additionally, electronic or vibrational states that are associated with defects, impurities, or surface phenomenon such as diffuse electron scattering, plasmons, and polaritons can be excited [22].

The time it takes for the excited electronic states to transfer energy to phonons and thermalize depends on the specific material and the specific mechanisms within the materials. For most metals, this thermalization time is on the order of 10^{-12}–10^{-10} s, whereas in non-metals, there is significantly more variation in the absorption mechanisms and the thermalization time can be as long as 10^{-6} s [7]. Polymers and dielectric materials are typically on the slower end of this range. Defects and quantum confined electronic states can play a significant role in slowing down this thermalization time.

When the laser-induced excitation rate is low in comparison to the thermalization rate, the details of the transient electronically excited states are not significant. Rather, one can consider the absorbed laser energy as being directly transformed into heat. Such processes are called photothermal (pyrolytic) and the material response can be treated in a purely thermal way. For instance, laser processing of metals or semiconductors with laser pulse times that are slow ($> ns$) is typically characterized by photothermal mechanisms.

When the laser induced excitation rate is high in comparison to the thermalization rate, large excitations can build up in the intermediary states. These excitation energies can be sufficient to directly break bonds (photo-decomposition). This type of non-thermal material modification is typically referred to as photochemical (photolytic) processing. During purely photochemical processing, the temperature of the system remains relatively unchanged. Irradiation of polymers with short

wavelength laser light, where the photon energy is on the order of the chemical bond energy, is an example of a photochemical processing. Similarly, ultrafast femtosecond laser pulses can enable photochemical processing of metals and semiconductors [28]. However, even in these cases, it is possible for thermal modifications to occur after the excited states thermalize with lattice phonons [30]. Material responses that exhibit both thermal and non-thermal mechanisms are typically referred to as photophysical [7].

4.2.3 The Heat Equation

For photothermal processing, the material response can be explained as a result of elevated temperatures. Therefore, it is important to be able to model the flow of heat inside a material. The temporal and spatial evolution of the temperature field inside a material are governed by the heat equation. The heat equation is derived from the conservation of energy and Fourier's law of heat conduction, which states that the local heat flux is proportional to the negative of the gradient of the temperature. In a coordinate system that is fixed with the laser beam, the heat equation can be written as [7]:

$$\rho\left(\mathbf{x},T\right)c_{\rho}\left(\mathbf{x},T\right)\frac{\partial T\left(\mathbf{x},t\right)}{\partial t}-\nabla\left[\kappa\left(\mathbf{x},T\right)\nabla T\left(\mathbf{x},t\right)\right]$$
$$+\rho\left(\mathbf{x},T\right)c_{\rho}\left(\mathbf{x},T\right)\mathbf{v}_{s}\nabla T\left(\mathbf{x},t\right)=Q\left(\mathbf{x},t\right) \tag{4.5}$$

where ρ is the mass density, c_p is the specific heat at constant pressure, κ is the thermal conductivity, and $\mathbf{v}_s$ is the velocity of the substrate relative to the heat source. The left hand side describes the evolution of temperature due to heat conduction as well as the convective term $\mathbf{v}_s$ to account for the shift in reference frame. In many laser processing applications, a laser beam is rastered across the work piece or some form of motion control is utilized to move the substrate relative to the beam. Therefore, this form yields a convenient transformations with which to deal with these issues. The right side incorporates the contribution of heat sources and sinks through the volumetric heating rate $Q\left(\mathbf{x},t\right)$.

The evolution of the temperature inside the material is initially driven by the volumetric heating term $Q\left(\mathbf{x},t\right)$ as well as the boundary conditions of the particular problem. Heat exchanges due to convection and radiation at the surface can be accounted for in the boundary conditions of the particular problem. In most cases, laser irradiation is the main source of volumetric heating. In general, for complex beam profiles, one would first have to solve the wave equation for the entire spatial intensity distribution of the light within the material, then take the magnitude of the gradient of intensity as the volumetric heating rate due to laser absorption as input into the heat equation. However, for the case of shallow surface absorption, this contribution can approximately be separated into a spatial shape $g\left(x,y\right)$ determined by the beam's profile, an attenuation term $f\left(z\right)$ determined from (4.4), as well as a

temporal shape $q(t)$, which could be a constant for CW, a pulse, or even a train of temporally shaped pulses. Phase changes or chemical reactions can be accounted for by $U(\mathbf{x}, t)$ and the volumetric heating term becomes,

$$Q(\mathbf{x}, t) = g(x, y) f(z) q(t) + U(\mathbf{x}, t) \tag{4.6}$$

In general, the heat equation (4.5) is a non-linear partial differential equation, which makes finding an analytic solution difficult. The situation is further complicated in real material systems due to changes in the optical properties (and hence the volumetric heating term) as a function of temperature and laser intensity. Thus, quantitative information generally requires methods such as finite difference or finite element numerical analysis. In some cases of extremely rapid material heating or very small material dimensions, the continuum assumptions of (4.5) may break down during the initial laser-material interaction requiring alternative modeling such as molecular dynamic simulations [31]. However, in most cases, shortly after the initial interaction, the heat equation regains its validity. In certain cases, there are simplifying assumptions that can be applied to enable analytic solutions, such as treating material properties as constants, incorporating laser heating through the boundary conditions for the case of surface absorption, or treating the laser shape term as a delta function for the case of a tightly focused laser spot. Solutions of this type can be found in standard textbooks on the subject [7, 8].

An important quantity that comes out of these simplified treatments is the thermal diffusion length $l_T \approx \zeta\sqrt{D\tau}$, where $D = \kappa/\rho c_p$ is the thermal diffusivity of the material. The thermal diffusion length characterizes the distance over which temperature changes propagate in some characteristic time τ. The prefactor ζ is a geometric constant on the order of unity, which depends on the particular geometry of the problem (i.e., bulk versus thin film absorption). Typically, τ is considered to be the laser beam dwell time or temporal pulse width, in which case we can consider the thermal diffusion length as a measure of how far the energy spreads during the laser irradiation. Following this initial interaction, further thermal propagation leads to elevated temperatures at distances beyond this length. The spread in energy during the laser pulse combined with the spread in energy after the pulse can lead to changes in the material properties. The region over which these changes occur is denoted the heat affected zone (HAZ), as discussed in the next section, and can exhibit a number of significant differences relative to the bulk material.

Given the preceding treatment of laser absorption, yielding the optical absorption depth, and the heat transport equations, yielding the thermal diffusion length, we can begin to clearly see the importance of lasers for surface modifications and the ways in which to control these interactions. For opaque materials, optical absorption depths are very small. With short laser dwell times, the thermal diffusion length is similarly small. In such a case, we are in a regime for which we may consider all of the optical energy as absorbed at the surface with a spatial profile matching that of the beam and without significant thermal diffusion out of this region during the initial interaction. Additionally, this confinement can be relaxed by increasing the absorption and diffusion lengths through the appropriate choice

of laser wavelength and increased dwell time. In this way, there is a great deal of flexibility in designing laser processes in order to achieve the exact desired material outcome.

4.2.4 Material Response

The details of the material response will depend on the particular material system and the laser processing conditions. As was mentioned earlier, if laser induced excitation rates are slow compared to the thermalization time, then the process is denoted as photothermal, and one can consider the absorbed laser energy as being directly transformed into heat. In this case, the material response will be a function of the local material heating and cooling rates, maximum temperatures reached, and temperature gradients, all of which can be determined from the solution to the heat equation for the given irradiation conditions. Because material heating rates can be so extreme, reaching as high as 10^9 K/s for nanosecond (ns) pulses and even higher for femtosecond lasers, significant changes to the material can occur.

In this section, we will discuss some of the fundamental material responses that can occur as a result of laser irradiation. The focus will be placed on photothermal responses, but attention will be drawn to photochemical aspects when necessary.

4.2.4.1 Thermally Activated Processes

Laser heating with fluences below the threshold of melting can activate a variety of temperature dependent processes within the solid material. The high temperatures generated can enhance diffusion rates promoting impurity doping, the reorganization of the crystal structure [32], and sintering of porous materials [33]. Energy barriers for chemical reactions can be overcome as well, increasing their reaction kinetics far beyond room temperature rates. Rapid transformations to high-temperature crystal phases can occur. The large temperature gradients achieved with localized laser heating can lead to rapid self-quenching of the material, trapping in highly non-equilibrium structures. Also, the rapid generation of large temperature gradients can induce thermal stresses and thermoelastic excitation of acoustic waves [34]. These stresses can contribute to the mechanical response of the material such as work hardening, warping, or cracking.

4.2.4.2 Surface Melting

Fluences above the threshold of melting can lead to the formation of transient pools of molten material on the surface. The molten material will support much higher atomic mobilities and solubilities than in the solid phase, resulting in rapid material homogenization. High self-quenching rates with solidification front velocities up to

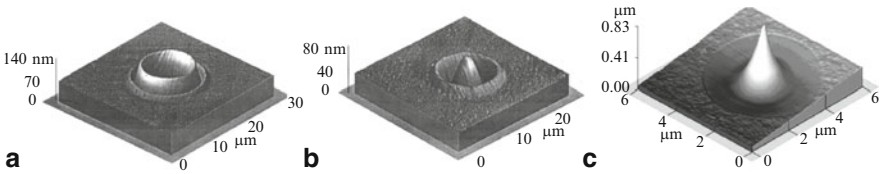

Fig. 4.2 AFM images of the surface deformations recorded on Ni-P hard-disk substrate at (**a**) high energy and (**b**) intermediate energy [38] and (**c**) 0.8 μm nanotips formed on Si SOI [39]

several m/s can be achieved by rapid dissipation of heat into the cooler surrounding bulk material [8, 9]. Such rapid quenching can freeze in defects and supersaturated solutes [35] as well as form metastable material phases. Slower resolidification rates can allow recrystallization of larger grains than the original material. Use of shaped beam profiles has also been shown to allow control of the recrystallization dynamics [36].

At temperatures far above the melting temperature, hydrodynamic motion can reshape and redistribute material. Radial temperature gradients on the order of $10^2 - 10^4$ K/mm can develop in melt pools, causing convective flows to circulate material [9]. For most materials, the liquid's surface tension decreases with increasing temperature and the liquid is pulled from the hotter to the cooler regions (Marangoni effect) [37]. Convective and thermocapillary forces can cause significant deformations that are frozen in during solidification. As can be seen in Fig. 4.2, a variety of shapes can form such as rimmed indentations, sombrero shaped craters, and even nanometer scale tips [38, 39].

4.2.4.3 Ablation

Laser ablation is the removal of material from a substrate by direct absorption of laser energy. Laser ablation is usually discussed in the context of pulsed lasers; however, it is also possible with intense CW irradiation. The onset of ablation occurs above a threshold fluence, which will depend on the absorption mechanism, particular material properties, microstructure, morphology, the presence of defects, and on laser parameters such as wavelength and pulse duration. Typical threshold fluences for metals are between 1 and 10 J/cm^2, for inorganic insulators between 0.5 and 2 J/cm^2, and for organic materials between 0.1 and 1 J/cm^2 [7]. With multiple pulses, the ablation thresholds may decrease due to accumulation of defects. Above the ablation threshold, thickness or volume of material removed per pulse typically shows a logarithmic increase with fluence according to the Beer–Lambert law (4.4).

A variety of mechanisms for material removal may be active during laser ablation depending on the particular material system and laser processing parameters such as wavelength, fluence, and pulse length [40]. At low fluences, photothermal mechanisms for ablation include material evaporation and sublimation. For multicomponent systems, the more volatile species may be depleted more rapidly,

changing the chemical composition of the remaining material [41]. With higher fluence, heterogeneous nucleation of vapor bubbles leads to normal boiling. If material heating is sufficiently rapid for the material to approach its thermodynamic critical temperature, rapid homogenous nucleation and expansion of vapor bubbles lead to explosive boiling (phase explosion) carrying off solid and liquid material fragments [42]. These thermal mechanisms can be understood as thermodynamic phase changes in response to the high temperatures.

When the excitation time is shorter than the thermalization time in the material, non-thermal, photochemical ablation mechanisms can occur. For instance, with ultrafast pulses, direct ionization and the formation of dense electron-hole plasmas can lead to athermal phase transformations, direct bond-breaking, and explosive disintegration of the lattice through electronic repulsion (Coulomb explosion) [43]. In certain nonmetals such as polymers and biological materials with relatively long thermalization times, photochemical ablation can still occur with short wavelength nanosecond lasers, producing well defined ablated regions with small HAZs [44].

In all cases, material removal is accompanied by a highly directed plume ejected from the irradiated zone. The dense vapor plume may contain solid and liquid clusters of material. At high intensities, a significant fraction of the species may become ionized, producing a plasma. Also, with pulses longer than ps, interaction of the laser light with the plume may be significant. The plume can absorb and scatter radiation, changing the actual flux received by the surface. Recoil from the plume can generate shockwaves in the material, causing plastic deformation and work hardening [45]. The recoil can also cause further expulsion of any remaining molten material as well as initiate shock waves. Resolidification of expelled liquid and condensation of plume material into thin films and clusters of nanoparticles [46] can alter the topography at the rim and surrounding areas of the ablated region (Fig. 4.3c, d).

The laser's temporal pulse length can have a significant effect on the dynamics of the ablation process. In general, as the pulse length is shortened, energy is more rapidly deposited into the material leading to a more rapid material ejection. The volume of material that is directly excited by the laser has less time to transfer energy to the surrounding material before being ejected. Therefore, the ablated volume becomes more precisely defined by the laser's spatial profile and optical penetration depth, and the remaining material has less residual energy, which reduces the

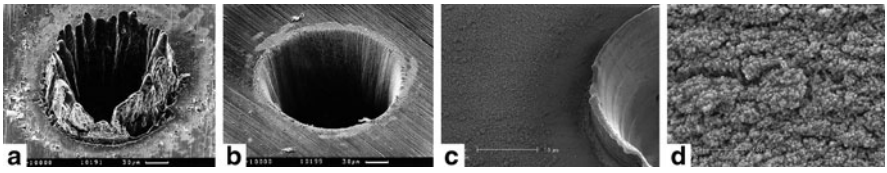

Fig. 4.3 Laser ablation of holes drilled in a 100 μm thick steel foil with (**a**) 200 fs, 120 μJ, $F = 0.5\text{J/cm}^2$ laser pulses at 780 nm; and (**b**) 3.3 ns, 1 mJ, and $F = 4.2\,\text{J/cm}^2$ laser pulses at 780 nm [28]. (**c**) Excimer laser ablation (300 pulses at 193-nm) of zirconium silicate (**d**) producing vapor-condensed aggregates of nanoparticles in the surrounding regions [47]

HAZ [48]. The effect of short pulses (fs to ps) is most apparent in the ablation of metals, which due to their large thermal diffusivities and low melting temperatures will exhibit large HAZs and molten regions when ablated with ns laser pulses. Figure 4.3 shows the relatively large molten layer present in the (a) ns irradiation of steel, in contrast to the precise ablation with (b) fs irradiation showing no trace of molten material [28]. The ablation threshold fluence for a material reduces at shorter pulse lengths and becomes more sharply defined. However, even for these ultrashort pulses, there is excess energy remaining in the material that can still cause thermal effects in the surrounding material after the pulse has ended [30]. Additionally, fs pulses can cause optical breakdown, which reduces the optical absorption depth and can even cause strong absorption in otherwise transparent wide-bandgap materials. Another distinction of fs and ps ablation is that the laser–material interaction is separated in time from material response and ejection. During ns ablation, shielding of the surface by the ejected ablation plume can reduce the amount of energy absorbed by the material.

Material responses often involve a combination of ablation, surface melting, and thermally activated processes, which can lead to cumulative changes in the material's surface texture, morphology, and chemistry. For instance, residual heat left after ablating material from a surface can lead to further melting or other thermally activated processes in the remaining surface and surrounding volume of material. These collective effects can result in complex multiscale material modifications, which can be utilized by various laser material processing applications. These applications will be discussed in the subsequent sections.

4.3 Laser Surface Processing Applications

In the previous section, we discussed some of the fundamental material responses that can occur in a material due to laser irradiation. These responses typically result in permanent changes to the material's surface chemistry, composition, crystal structure, and morphology. By choosing the appropriate laser parameters, precise control of the final material properties can be achieved. This enables processing procedures to be designed and optimized to provide the best material functionality for its desired application. In this section, we briefly discuss some examples of established applications for laser processing. For a more thorough treatment of the details and applications of these laser surface processes as well a mathematical models describing behavior and dependence on processing parameters, the reader is encouraged to follow references [6–9].

One of the first production applications for lasers in surface material processing was the selective heat treatment of metallic parts for reduced wear [4]. Traditionally, heat treatment of metals involved heating in an oven, flame, by induction, or electric arc above a critical temperature to achieve a crystal phase transformation and then subsequently quenching in a gas or liquid to rapidly cool to room temperature and

freeze in a non-equilibrium phase. The rate of cooling from the high temperature crystal phase determines the resulting room-temperature crystal morphology and mechanical properties. Such heat treatments are commonly used to harden or temper load-bearing surfaces for reduced wear, decreased friction, and increased part lifetime [49]. However, in many cases, it is undesirable to treat the entire part as it may be prone to distortion or cracking. By using a laser, rapid heating of the surface can be achieved with little thermal penetration. Subsequent self-quenching into the cooler bulk enables modification that is limited to a thin layer of surface material. The heating and quench rates, and thus resulting material properties, can be precisely controlled by adjusting laser parameters such as pulse time (or scan speed for CW lasers) and intensity [32]. The major advantages of laser surface heat treatment include high processing speeds, precise hardening depth control, minimization of part distortion and cracking, elimination of separate quenching medium, and the ability to selectively harden small hard to reach areas (e.g., inside surface of small holes).

Much like laser hardening, non-melt laser annealing (NLA) utilizes rapid surface heating to enhance atomic mobilities and reorganize the crystal structure. NLA is commonly used to activate the diffusion of ion implanted dopants in silicon wafers to disperse undesirable clustering and repair the lattice damage created during the implantation process [50]. The short thermal penetration and lack of melting allow processing of shallow junctions while preserving composition gradients. On the other hand, excimer laser annealing (ELA) utilizes melting in a thin layer of material at the surface, which then rapidly recrystallizes to relieve internal stresses, remove defects, and enhance crystallinity. ELA is crucial to the production of high-performance, large-area polycrystalline silicon (poly-Si) thin-film transistor (TFT) devices such as active-matrix-driven flat panel displays [26]. ELA is used to recrystallize poorly conducting amorphous silicon to produce larger grain sizes and reduce defects. ELA has also been used in the production of poly-Si thin films for solar cells.

Laser surface melting can also be used to incorporate new material into an existing surface. In laser cladding and hardfacing, new material is fed in by wire feedstock or as a blown powder and bonded, ideally without dilution, to an underlying substrate to create a new surface with little to no porosity and enhanced resistance to wear, high temperature, and corrosive environments (Fig. 4.4a). It provides coatings with a more consistent thickness, better surface finish, smaller HAZs, less cracking, and reduced part distortion than traditional thermal spraying and welding techniques. With higher laser power, complete mixing of the new material into the molten surface can form a homogenously alloyed layer. Rapid resolidification ensures minimal segregation, allowing many materials to be alloyed regardless of their mutual solubility [8]. Materials can be alloyed to increase their hardness and corrosion resistance or reduce friction wear properties of the part surface.

Laser cleaning utilizes intense laser radiation to selectively remove contaminants from a solid surface while leaving the underlying substrate largely unaffected. The technique exploits differences in the optical and thermal properties of the underlying substrate and the contaminant layer as well as the ability to precisely control

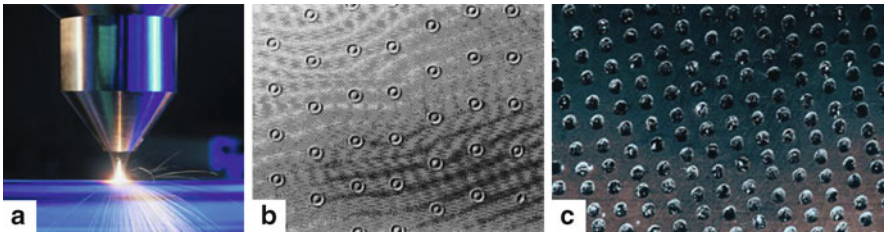

Fig. 4.4 (**a**) Laser surface cladding (MTU Maintenance). (**b**) Micrograph of laser-textured bumps on a super-smooth disk as observed in a phase-contrast microscope [51]. (**c**) Laser surface texturing of micro-dimples for enhanced tribology [52]

material heating depths and removal rates by controlling laser beam parameters such as pulse time (or scan rate), wavelength, and fluence (or intensity). Laser cleaning has become a cost effective alternative to water jet, abrasive blasting, or chemical based cleaning methods. Typical industrial applications include oxide and coating removal, tool cleaning, removal of grease and paint, as well as adhesion promoting pre-treatments for welding, gluing, and painting. Laser cleaning can also be used to efficiently remove very small particles from delicate substrates such as silicon wafers and photolithographic masks [7, 53].

Finally, one of the most important and technologically relevant laser surface processing applications is surface texturing. Laser surface texturing has historically been used to enhance the tribological properties of material interfaces. For instance, magnetic disk drives require surface texturing to overcome stiction problems and reduce friction (Fig. 4.4b) [54]. Also, laser surface texturing of microscopic dimples can improve material tribology by serving as micro-hydrodynamic bearings, micro-reservoirs for lubricant, or micro-traps for wear debris (Fig. 4.4c) [5]. In other cases, texturing can be used to improve adhesion of mating surfaces. Laser textured rollers are commonly used in the manufacturing and processing of flat-rolled steels in the automobile industry to increase the grip on the steel sheet and impart a matte finish to enhance formability and improve the adhesion and appearance of paint [2, 8].

A more recent development in surface texturing involves the creation of superhydrophobic surfaces ($\theta_c > 150°$) for applications such as self-cleaning surfaces, biological scaffolds, microfluidics, and lab-on-chip devices [56–59]. The process is inspired by several examples from nature, most notably that of the lotus leaf, where natural surface textures result in exceptional water repelling properties (Fig. 4.5a) [60]. The effectiveness of these natural textures is due to the multiscale nature of the features that ranges from the nano- to the microscale [61]. Figure 4.5b shows a close-up image of the surface of a lotus leaf indicating nanotexture on microscale-pillars. Laser texturing can mimic these multiscale structures (Fig. 4.5c) and their superhydrophobic properties (Fig. 4.5d) with a large degree of control through the choice of processing parameters [59]. For example, by varying laser fluence, surface wettability gradients can be generated to drive microfluidic flows [58].

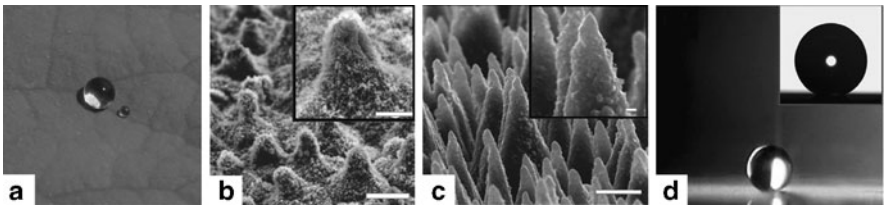

Fig. 4.5 (**a**) A bead of water on a lotus leaf [55]. (**b**) SEM image of the microscale (scale bar 10 μm) and *inset*: nanoscale structures (scale bar 5 μm) on the surface of a lotus leaf [56]. (**c**) SEM images of femtosecond laser textured Si surface showing microscale (scale bar 5 μm) and *inset*: nanoscale (scale bar 1 μm) structures [56]. (**d**) Image of a water droplet on a laser-structured, silane-coated, Si surface with a static contact angle of $\theta = 154 \pm 1^\circ$ [57]

Laser surface processing excels over mechanical (e.g., shot or grit blasting), chemical, and electric discharge texturing because it allows localized modifications with a large degree of control over the shape and size of the features that are formed and a greater range of sizes that can be produced. It is generally cheaper than e-beam texturing and more flexible in that it does not require vacuum. Various textures can be accurately produced (Figs. 4.2, 4.3 and 4.4 b, c) by controlling processing parameters such as beam intensity, spatial and temporal profile, wavelength, and processing environment (background gas or liquid). The primary dimensions of the surface features (e.g., width of the melted or ablation region) are generally defined by the shape and size of the beam. However, secondary microscale and even nanoscale features can form in and around the irradiated region due to a variety of mechanisms including post-ablation melting and resolidification or splashing of a liquid surface due to the recoil pressure as discussed above. These secondary characteristics can be just as important as the primary dimensions in determining material functionality in its desired application.

In the next sections, we present two case studies where laser processing has been used to control the multiscale texture of a material surface as well as influence its surface chemistry and composition in order to optimize material performance. The first application utilizes laser surface texturing to enhance the absorption of light by semiconductor devices for improved efficiency. The second looks at the use of laser texturing to modify the cellular response and adhesion to biological implants.

4.4 Case Study I: Surface Texturing for Enhanced Optical Properties

A large number of important applications rely on semiconductor devices to convert light into an electrical response. For instance, photovoltaic arrays are used to convert solar radiation into renewable electricity, mitigating our reliance on fossil fuels. Photodiodes are widely used in optical communication, optical data storage, or chemical sensing to transduce an optical signal into an electrical one. Digital

imaging sensors have continued to replace film in consumer cameras and have enabled machine vision to automate many industrial operations. Optimum performance in all of these applications requires the optical device to capture as much of the incident light as possible. In this case study, we will discuss how laser texturing of semiconductor surfaces can be utilized to decrease reflections and increase absorption for enhanced device performance without altering bulk properties.

At the heart of the optical to electronic energy conversion in a semiconductor device is the absorption of light by the mechanisms discussed in the earlier sections. Light enters through the air–material interface, where a discontinuity in the index of refraction causes a portion of the wave to reflect and carry off a fraction of the incident power equal to the reflectivity (4.3). Because of the high index of refraction of most semiconductors, this parasitic Fresnel reflection (e.g., 30% for silicon and 25% for CdTe) can significantly reduce the optical power available for transduction into an electrical response.

The most common solution is to apply a single-layer, thin-film antireflection coating [62]; however, such coatings are effective only in a narrow spectral range and at normal incidence. Broadband reduction in reflectivity over a larger range of incidence angles can be achieved with multilayer and graded index (GRIN) thin films. However, their application tends to be costly and the availability of coating materials with the appropriate physical and optical properties is limited [63].

An alternative method for the reduction of reflections is to texture the existing semiconductor surface. Because no additional material is added, these textured surfaces are inherently more stable and do not suffer from material compatibility issues that plague thin films such as weak adhesion, thermal expansion mismatch, and interdiffusion.

Multiscale texturing of a surface can cause significant deviations in how light is reflected and scattered, leading to enhanced absorption over that of a flat smooth surface. For surface features with dimensions greater than several wavelengths of light, this enhancement can most easily be described using the principles of ray optics. A portion from a ray of light will specularly reflect from a flat surface, as shown in Fig. 4.6a, and have no further interaction with the material. On the other hand, protruding features can reflect and scatter light back onto the surface, as seen in Fig. 4.6b. Light can effectively become trapped in crevices and holes where multiple reflections enhance the coupling into the material. Once inside these protruded structures, multiple internal reflections can guide the light into the bulk. Refraction at the surface of these structures also leads to transmission at oblique angles, effectively increasing the optical path length, enhancing absorption. The degree of enhancement depends on the particular geometry and dimension of the surface features [1].

The creation of features at or near the surface with dimensions on the order of a wavelength (e.g., cracks, voids, surface roughness) can also affect the surface reflectivity by scattering light in the material and increasing the optical path length, leading to enhanced absorption. This is especially important for enhancing absorption in thin-film devices where the thickness of the film is on the order of the optical wavelength [64].

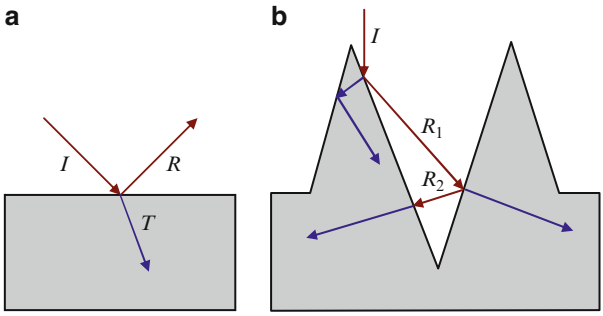

Fig. 4.6 (**a**) Light specularly reflecting from a flat surface. (**b**) Multiple reflections from protruding structures enhance coupling into the material, and refraction causes the light to prorogate at oblique angles, increasing the optical path length

Table 4.1 Multiple length scales over which reflectivity and absorption is determined by surface features

Feature size	Influence on reflectivity
$\gg \lambda$	Light trapping due to multiple reflections enhances coupling into the material. Light refracted at oblique angles increases the effective optical path length
$\approx \lambda$	Small features can successively scatter light, increasing the effective optical path length and enhancing absorption
$\ll \lambda$	Subwavelength structures (SWS) can reduce reflections through the moth-eye effect

Moving still smaller, surface features with dimensions much smaller than a wavelength are not individually resolved by the light, yet periodic arrays of subwavelength structures (SWS) can contribute significantly to the optical response. This is commonly known as the “moth-eye effect," as it was first discovered by Bernhard [65], who found that tapered nanostructures were responsible for the antireflection camoflauge of a moth’s eye. A simple explanation for this phenomenon is that the medium takes on a volumetric average of the optical properties between that of the material and the surrounding medium [63, 66]. The tapered nanostructures therefore cause the effective optical properties to continuously change from that of air to that of the material, essentially acting as a GRIN antireflecting layer.

The breadth of length scales over which surface texture affects reflectivity, as summarized in Table 4.1, indicates that surface texturing over multiple length scales can lead to significant reductions in reflectivity and can enhance the absorption of light by the material.

A variety of techniques have been utilized to texture a material’s surface to enhance its absorption. Most commercial single crystalline solar cells are etched with potassium hydroxide to enhance light trapping [67], but the texture is limited to random pyramidal structures and the anisotropic etching does not apply to polycrystalline materials. Lithographic techniques combined with isotropic etching have been used to accurately define arbitrary nanoscale patterns to engineer opaque materials such as “black silicon" [68]; however, these processes would be too costly

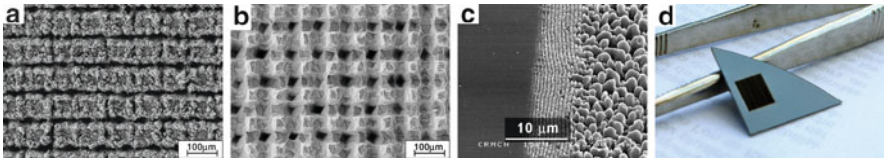

Fig. 4.7 SEM images of multicrystalline silicon direct-write surface textured with a rastered beam (**a**) before and (**b**) after etching to remove laser-induced damage [72]. (**c**) SEM image of silicon processed in vacuum with 800 nm, 100 fs pulses. The remnants of LIPSS with periodicity equal to the laser wavelength can be seen at the edge of the irradiated region (*center*) which transitions to beads approximately 2 μm in width (*right*) [73]. (**d**) Square region of a silicon wafer textured with spontaneously forming quasi-periodic microstructures appears black in contrast to the unprocessed regions [73]

to apply to mass production [66]. Other techniques such as mechanical scribing [69] and solution based pattern deposition [63] have been investigated but may be difficult to integrate into certain manufacturing processes. In contrast, laser texturing is a non-contact technique which can be utilized on both crystalline and polycrystalline material.

There are two distinct methodologies which have been investigated for laser texturing surfaces to enhance absorption. The first is direct-write micromachining where a focused beam is scanned across a surface in a pattern to selectively ablate material and define the structures [21] (Chaps. 10 and 11). It has been used to texture pits, grooves, and pyramidal structures in mono and polycrystalline silicon to enhance absorption (Fig. 4.7a, b) [70–72]. Laser direct write allows a great deal of flexibility in defining surface texture; however, feature dimensions are limited by the focus size of the beam. The second laser texturing methodology is based on spontaneously forming quasi-periodic microstructures, which have been observed on laser exposed surfaces. Under the right conditions, arrays of high-aspect-ratio features such as cones or pillars will fill the irradiated regions of the surface. Surfaces textured in this manner exhibit some of the highest increases in absorptance over a wider spectral band than surfaces textured by the other techniques. And unlike direct writing, large areas can be textured at once by using an unfocused beam. Therefore, there has been a lot of interest in understanding how these structures form and their dependence on processing parameters in order to optimize the processing for cost effective integration into the commercial mass production of semiconductor devices.

The spontaneous formation of laser-induced periodic surface structures (LIPSS) has been studied extensively since the 1960s. Shallow surface rippling with a period close to that of the laser wavelength was first reported by Birnbaum [74] using a ruby laser and has since been identified as a universal phenomenon observed on a variety of materials irradiated above their melting threshold [75]. These ripples, now referred to as low spatial frequency LIPSS (LSFL), are generally well understood and are attributed to interference between the incident beam and a surface scattered wave resulting in an inhomogeneous energy deposition [76, 77]. Recently, structures with subwavelength spatial periods as small as $\lambda/6$ have been observed on

material surfaces irradiated with multiple ultrashort laser pulses. These high spatial frequency LIPPS (HSFL) are generally observed for fs excitation in the transparency range of the material; however, they have also been reported for above-band gap fs excitation of semiconductors and metals. The formation mechanisms of the HSFL remain a topic of debate in the current literature and explanations include nonlinear interactions, transient optical properties during irradiation, self-organization, and Coulombic explosion [78, 79].

The effects of LIPSS on surface optical properties have been noted as acting like a surface grating and have been shown to exhibit dispersive reflections [80]. However, due to their shallow height, they do not significantly contribute to the material's absorptance. Irradiation with a higher fluence near or above the ablation threshold, such as that during pulsed-laser deposition, has been found to lead to surface roughening with larger scale features such as mounds or small mountains [81]. For instance, Fig. 4.7c shows LIPSS at the edge of a laser irradiated region of silicon which transitions into larger bead-like structures. With a large number of additional pulses, reflections from the sides of these features will concentrate light into the surrounding valleys, activating a positive feedback mechanism where material is removed from the valleys and partially deposited onto the peaks. This can lead to the formation of high-aspect-ratio features such as cones or columns [82]. These structures are highly efficient at trapping light and suppressing reflections. Figure 4.7d shows the laser-textured square region of a silicon wafer, which appears black in contrast to the highly reflecting unprocessed regions. In addition, these surfaces have a profound effect on the hydrophobicity of the surface as discussed in the previous section (Fig. 4.5). These structures have been observed on a variety of materials including Ge, W, Ti, Ta, Mo, Pt, steel, and NiTi alloy [83–86]. However, most systematic studies have focused on silicon because of its technological importance.

There is still debate over the mechanism by which these initial undulations form and subsequently transform into cones or columns [87–93]. However, the nature of the process and the details of the final microstructure, such as the shape of the cones or columns, their regularity and density on the surface, chemical composition, and presence of nanostructure, depend strongly on the variables involved in the processing such as the number of incident laser pulses, laser fluence, wavelength, pulse duration, as well as the ambient environment. The structures align with the direction of laser-beam propagation with little dependence on the surface normal and crystallographic orientations. The use of linearly polarized light causes the base of the structures to be elongated perpendicular to the axis of polarization which is consistent with the greater reflectivity and decreased absorption of *s*-polarized light. Also, the size, aspect ratio, and spacing of the microstructures increase with increasing laser fluence. Figure 4.8a, b show SEM images of silicon irradiated with a Gaussian beam producing microstructures with local density and size reflecting the variation of fluence across the laser profile [94].

Processing atmosphere plays an important role in determining the formation mechanisms and microstructure of the silicon surface. Her et al. found that silicon processed in vacuum, He, and N_2 produced blunted structures as shown in Fig. 4.8a, whereas SF_6 and Cl_2 environments produce conical or triangular sharp spikes with

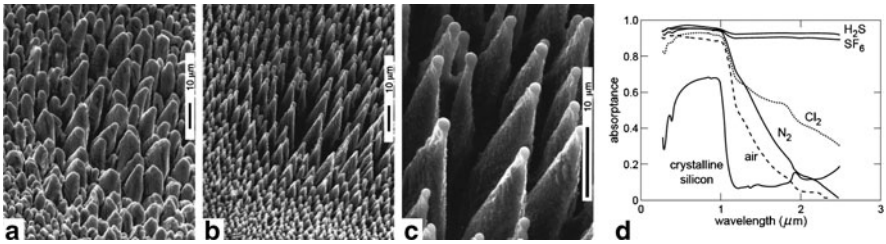

Fig. 4.8 SEM images of the surface microstructuring of Si(100) by 500 laser pulses of a 200 mm diameter, nearly Gaussian beam (100-fs, 800 nm, 10 kJ/m^2) (**a**) processed in vacuum and (**b**,**c**) in a 500 Torr atmosphere of SF_6. Images viewed at an angle of 45° from the surface normal [94]. (**d**) Absorptance of femtosecond laser microstructured silicon in a variety of gases [95]

spherical caps (Fig. 4.8b, c) [94]. The difference was attributed to laser-induced plasma etching by the halogen-containing gases. Nearly identical spiked structures were produced with H_2S indicating the importance of sulfur in the etching process [95]. Younkin et al. found that the number density of structures created was greatest in SF_6, slightly more than Cl_2, but approximately twice that of N_2 and air. Processing in water with 400 nm irradiation produced submicrometer spikes while 800 nm irradiation only resulted in roughening and holes [96]. This strong dependence on wavelength is not observed for gaseous atmosphere or vacuum processing.

Processing environment also has a major impact on the optical properties of the microstructured surface. Figure 4.8d shows absorptance measurements of silicon microstructured in a variety of atmospheres. All of the gases show significant enhancement over the unstructured sample for light above the band gap (250 nm to 1.1 μm). This can be attributed to the microstructure's ability to trap light and reduce reflections. Beyond the band edge (1.1 μm–2.5 μm), the absorptance of N_2-, Cl_2-, and air-processed samples decreased continuously while SF_6- and H_2S-processed samples remained at about 90% absorbing [95]. It was suggested that damage to the lattice and alteration of the band structure through the incorporation of sulfur was responsible for the near unity absorptance in the infrared. Processing with other chalcogens, such as selenium and tellurium, also led to near-unity broadband absorption [3].

The temporal laser pulse width also has a noticeable effect on the formation mechanisms and resulting morphology. Crouch et al. found that despite similar near-unity broadband absorption, processing in SF_6 with fs pulses produced significantly different structures on the surface of silicon than ns pulses [97]. The fs-formed structures are about 8 μm tall with their tips level with the original surface, indicating that ablation and etching dominate the formation. They are also covered with nanoscale particles and features. The ns-formed structures are smoother, stand five times taller at 40 μm, and protrude from the original surface indicating that material deposition played a part in the growth process. Both cases produced structures with a crystalline silicon core covered with a highly disordered layer of nanocrystallites, nanopores,

and sulfur impurities. However, this layer was much thinner and more sparse on the ns-formed structures. They also concluded that the below-band gap enhancement in absorptance is due to an optically active sulfur configuration in the silicon, which degrades upon annealing.

In summary, multiscale texturing plays an important role in a material's optical properties, and such behavior can be exploited for applications such as photovoltaics or electron emitters. At the cutting edge of this is the laser structuring of silicon to produce a variant often referred to as black silicon. Such a structure has been shown to absorb 95% of incident radiation with energy above its bandgap [250–1,100 nm] [98]. Below the bandgap, in which unprocessed silicon is essentially transparent, the microstructured silicon absorbs 90% of incident radiation for wavelengths [1,100–2,500 nm]. This enhanced absorbance has resulted in high-sensitivity infrared photodetectors [99, 100], high-quantum-efficiency avalanche photodiodes (APDs) [101], and has even spawned a company taking advantage of the processing technology (SiOnyx).

4.5 Case Study II: Surface Texturing for Enhanced Biological Interactions

Biological implants are often utilized to reinforce or replace diseased or damaged tissue in the human body. For example, the implantation of a prosthetic joint or the replacement of a tooth are standard orthopedic surgical procedures used to relieve pain and regain functionality in order to improve the quality of life for the patient. Although these procedures are common and generally have a high success rate, fears about the limited implant lifetime have prevented the procedures from being fully utilized in all potential cases. For instance, the typical lifetime of a hip implant can be as short as 10–15 years requiring complex and costly retrieval and revision surgery to reattach the implant [102]. While recent advances in biomaterials engineering have limited the number of failures due to wear or fracture of the implant itself, loosening of the load bearing surfaces of the implants from the supporting hard tissue can still lead to malfunction [102, 103]. Abrasion between the loose implant and the bone surface can cause pain and further wear. Accumulation of debris particles can trigger a macrophage-induced inflammatory response that can lead to bone loss (osteolysis) and further implant loosening [104]. This damage can make future revisions of the implant more difficult and dangerous. Therefore, much of the current implant research has focused on engineering biomaterials that allow for rapid integration with the supporting hard tissue, resist loosening, and shorten the recovery period.

The difficulty faced by biomaterials engineers when designing load bearing implants is that there are a limited number of naturally biocompatible materials with the appropriate mechanical properties to sustain unencumbered, long-term loading in a biological environment. For example, Ti-6Al-4V (Ti64) is one of a few completely biocompatible materials and is the most common metal used in dental

and hip implants because of its excellent fracture toughness, fatigue resistance, and Young's Modulus near that of bone. With such exceptional bulk material properties, researchers now focus on implant surface engineering as a means to enhance the physiological response to existing biomaterials without degrading their bulk strength and weight properties. Biological cells and tissues mainly interact with the outermost atomic layers of an implant [105]. Therefore, modifying only the surface morphology and chemistry is sufficient to elicit novel biological responses from existing materials [102]. Laser processing is ideally suited to such an endeavor.

Current attempts to enhance implant longevity have focused on the initial stages of cell adhesion and osseointegration. Osseointegration is the process by which a direct structural and functional bond is formed between living bone and the surface of the artificial implant without intervening soft tissue. Initially, the surface of a newly fixed implant becomes conditioned by the adsorption of proteins (fibronectin, actin, vinculin, and integrins), which are active in cell adhesion, growth, and differentiation [106, 107]. Osseointegration is then initiated by the osteoblast cells, which migrate to the conditioned implant surface and proliferate in the voids that exist between the implant and the existing bone. The early activities of these osteoblast cells lay the groundwork for mature bone cells that will eventually be formed in that region [108]. It has been seen that surface texture and chemistry greatly influence the adsorption of protein and modify how the osteoblast and other cells attach and interact with the implant surface environment [102, 107, 109, 110]. Thus, optimizing these surface properties can increase the chances of successful osseointegration.

There are several relevant length scales over which modified surface topography and chemistry of a processed implant can influence cell adhesion and behavior, enhance osseointegration, and improve the resulting bond to existing bone [111, 112]. Modifying implant surface energy through chemical processing increases adhesion at the atomic scale and has been shown to improve bonding of proteins and cells [113]. Nanoscale surface features can affect protein interactions associated with cell signaling, which regulates cell adhesion, proliferation, and differentiation. Also, nanoscale surface features can influence the interactions of individual cell microfilaments and microtubules that form focal adhesion complexes (the protein complex that attaches the cell to the surface). Figure 4.9a shows osteoblast-like cells adhering to a surface with the focal adhesion points visible in green. Texturing with micron-sized features such as grooves, ridges, craters, and mountains can increase surface area and provide more opportunities for focal attachment. It can also cause cells to mechanically stretch or contract to align and organize with the features, a phenomenon known as 'contact guidance' (Fig. 4.9b) [111, 114, 115]. This alignment can be utilized to promote healthy regeneration of bone. Since bone consists of sheets of parallel cells, initiating bone healing with parallel cells may improve the healing process [116]. Also, cells grown on substrates with linear grooves exhibit organized regrowth, possibly decreasing scar tissue formation during healing [117]. Finally, macroscopic features textured on the surface of the implant such as vents, slots, dimples, and threads can physically interlock the implant with the bone, increasing longevity [118–121].

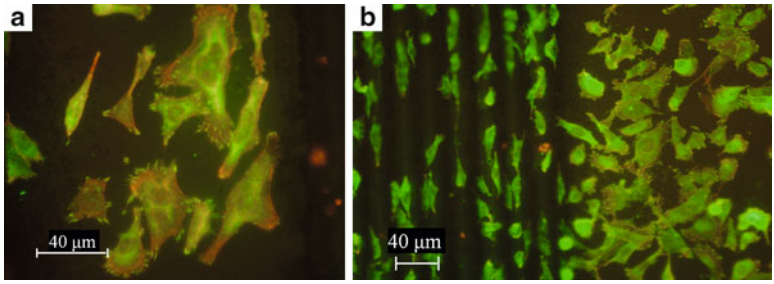

Fig. 4.9 (**a**) Osteoblast-like human osteosarcoma cells. Their vinculin and focal adhesion points are stained *green* and their actin stained *red*. (**b**) Contact guidance by linear grooves causes elongation of the cells (*left*) as compared to the adherance to a polished surface (*right*). (Images by Lara Ionescu)

Table 4.2 Multiple length scales over which the adhesion of bone to the implant is determined

Length scale	Influence on cell adhesion
Atomic scale	Surface energy controls the atomic bonding of proteins and cells
Nanoscale	Nanoscale surface features affect interactions of protein, cell microfilaments, and microtubules, which form focal adhesion complexes and cell signaling, which regulates cell adhesion, proliferation, and differentiation
Microscale	Micron-sized features such as grooves, ridges, craters, and mountains can increase surface area, provide more opportunities for focal attachment, and cause cells to mechanically stretch or contract to align and organize with the features (contact guidance)
Macroscale	Macroscopic features such as vents, slots, dimples, and threads can physically interlock the implant with the bone

Table 4.2 shows a breakdown of the relevant length scales and the biological–material interactions that occur on that scale. As we can see, osseointegration is inherently a multiscale issue, requiring control and understanding of surface properties over many different size scales. Laser surface texturing gives researchers a tool with which to rapidly and conveniently modify surfaces over these scales without the need for subsequent processing.

Various methods to modify biomaterial surface properties have been investigated. Chemical treatments and ion beam implantation have been used to alter surface composition and functionalization. Microprinting of patterned thiols, proteins, silanes, and polymers have also been demonstrated to modify biological adhesion and cellular response. Various biomaterial coating techniques such as liquid immersion, thermal spray, plasma spray, electrocrystallization, electrophoretic processes, and laser-assisted surface coating have been utilized to deposit thin layers of highly biocompatible yet brittle material onto a more rigid supporting material [122]. Such coatings have been shown highly effective at enhancing biocompatibility; however, they tend to require complicated preparation processes and still have problems with coating homogeneity and adhesion to the substrate. Alternatively, laser heat treatments do not share these difficulties associated with coatings as no additional

material is added to the surface. Yet at the same time, these methods allow for similar changes in wetting characteristics of the existing surface by changing roughness, microstructure, and surface chemistry of Ti-6Al-4V [123, 124], positively affecting corrosion resistance and biological adhesion.

Additionally, various techniques have been employed to texture the surface of implants. Currently, implant surfaces are roughened through randomized processes such as sand blasting (Al_2O_3 or SiC particles) or acid etching to encourage cell growth and improve osseointegration [125]. Such techniques are relatively inexpensive and easy to perform on complex surfaces, but cells that grow on these surface typically do so equiaxially leading to the development of random bone cell orientations [126]. Also imbedded blasting particles can contaminate the surface with increased concentrations of cytotoxic elements [127]. Other techniques such as ion beam and electron beam texturing have enabled precise control of complex features but require vacuum, which adds to the cost and limits the dimensions of implants that can be textured. Photolithography has also been used but requires complicated preparation processes and is limited in the implant geometries it can handle and in its ability to produce multiscale features [115].

Alternatively, laser surface texturing provides a fast, non-contact, and clean alternative for microstructuring in ambient conditions. Unlike lithographic techniques, it can handle irregular implant shapes. A number of studies have investigated laser machining of surface features to enhance cellular adhesion to biomaterial surfaces and improve resistance to implant loosening [116, 117, 122, 128–130]. However, most have focused on optimizing cellular response as a function of primary feature dimensions (groove width and depth, dimple diameter, etc.). As was discussed in the background section and previous case study, one of the key benefits of laser processing is the ability to modify surfaces over multiple lengths scales. For instance, Fig. 4.10a, b show a dental implant that was laser micro-patterned using a kinoform producing a regular array of dimples directly on its threads. Figure 4.10c shows a close up of an individual patterned dimple which reveals secondary features such as the presence of material redeposited on the rim and splattered into the surrounding area. This multiscale modification to the surface is critically important in determining the overall interaction between the cells and the surface. Different

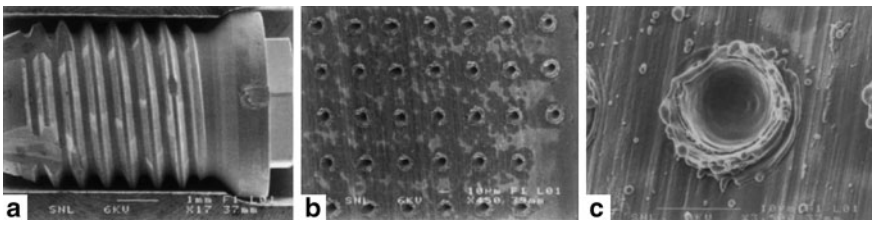

Fig. 4.10 (**a**) SEM image of a dental implant that was laser micro-patterned using a kinoform with (**b**) a regular array of dimples patterned directly onto its threads. (**c**) A close up of one of the 10 μm pits showing remnants of material resolidified on the rim and ejected into the surrounding region [128]

combinations of processing parameters (e.g., number of pulses, pulse energy, pulse time, spot size, laser frequency) can achieve the same primary feature dimensions but with different secondary features.

Ulerich et al. investigated the effects of multiscale laser texturing of a Ti-6Al-4V substrate on the adhesion of osteoblast cells [129]. They rastered a focused beam from a ns pulsed UV laser across the surface to pattern linear grooves. By manipulating processing parameters such as pulse energy, translation distance between pulses, number of passes over the same groove, and machining environment (air, water, or silicon oil), they were able to exercise a large degree of control over the groove properties. They found that groove width was not significantly affected by the number of passes or the distance between pulses. However, they found that they could accurately manipulate groove width by controlling the pulse energy. This control is explained by the fact that as pulse energy increases, a larger fraction of the Gaussian beam exceeded the ablation threshold. Groove depth, on the other hand, was affected by the translation distance and the number of passes as well as the laser pulse energy. Decreasing the distance between pulses or making multiple passes would increase groove depth without affecting the width. This allowed further control of the grove wall slope through selection of processing parameters. These findings are illustrated in Fig. 4.11, which shows cross sectional SEM images of the grooves obtained with different translation distance between pulses.

In addition to the primary groove characteristics, they found that processing conditions also affected the roughness and sub-micron features created on the surface. Small-scale features would form on the surface of the grooves depending on the specific nature of the material ablation and redeposition. Lower surface heating rates had the tendency to merely melt the surface with thermocapillarity causing a net change in the surface morphology, resulting in a smooth surface. As heating rates

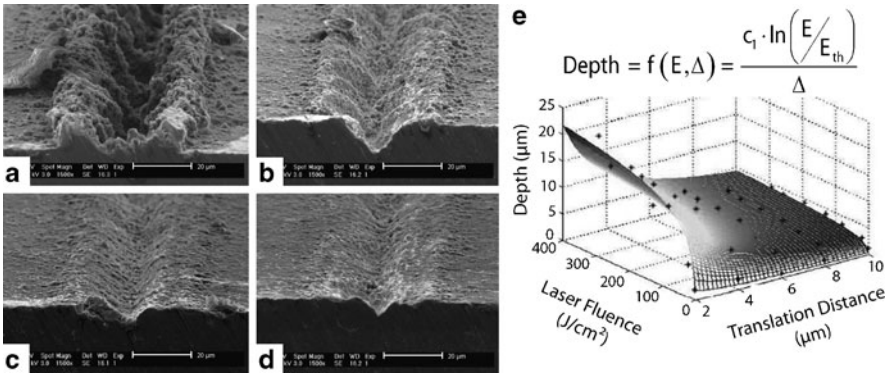

Fig. 4.11 Cross-sectional SEM images (scale bars are 20 μm) of the laser-machined (56 J/cm^2) surfaces shows decreasing size and slope of groove walls with increasing translation distance: (**a**) 2 μm, (**b**) 4 μm, (**c**) 6 μm, and (**d**) 8 μm. (**e**) Groove depth measurement as a function of translation distance and laser fluence [129]

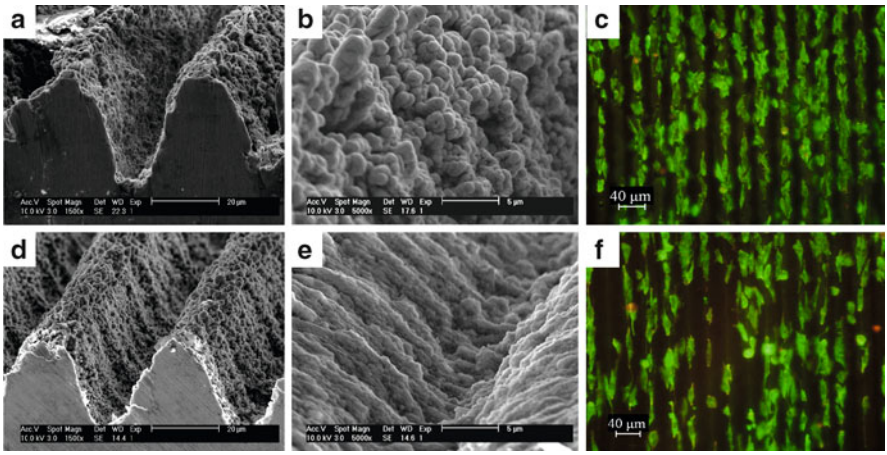

Fig. 4.12 The top (**a,b,c**) and bottom (**d,e,f**) structures have the same groove width and depth but different secondary features (**b** and **e**) resulting in different cellular adhesion behavior (**c** and **f**)

increased, recoil from ejected material would splatter material from the molten pool, which would recast in the surrounding regions with splatter patterns largely affected by the force with which they were expelled. Decreasing the translation distance between laser pulses had the tendency to increase surface roughness due to the increased interaction with the residual heat left from previous pulses. Using a dynamic set of machining parameters, they were able to intentionally create many sub-micron features including nodules, ripples, ledges, and nano-textures (Fig. 4.12b, e) [129].

Surface texturing of the Ti-6Al-4V substrate was also done in liquid environments (water and silicon oil), which enhanced the quenching rate of the laser heated material. Grooves machined in liquid environments tended to contain other types of features such as bubbles where pockets of liquid vaporized during the process. Cracking was also apparent on the surface of the liquid-machined grooves due to additional thermal stresses induced from the high quench rate.

Ulerich et al. found that the surface chemical composition was also affected by the laser texturing process. For instance, they found that with a small translation distance between pulses, there was a measurable depletion of aluminum in the valleys of the grooves and an enrichment of aluminum on the ridges. This effect is consistent with a transient molten pool at the bottom of the grove that preferentially evaporates aluminum due to its higher vapor pressure. In contrast, they found that the depletion of aluminum did not occur under liquid environments. Surface chemical composition can influence how cells attach and react to a metal by changing the way that proteins adsorb or by activating different cellular pathways with nearby cells. Additionally, when dealing with alloy materials, shifts in the surface chemistry can lead to an overabundance of cytotoxic elements on the surface or changes in the mechanical properties of the surface. Therefore consideration of chemical composition changes is important when designing implant processing procedures.

To probe the effects of surface structure and chemistry on the adhesion of cells, Ulerich et al. conducted fluorescent studies of live osteoblast cells cultured on the Ti-6Al-4V surfaces. Results such as these (Fig. 4.12) demonstrate that the direct-write laser-machined grooves led to contact guidance (cell alignment) as well as enhanced cell density with respect to the original surface when structured in an optimal fashion [131]. Also, through such studies, it is possible to probe the importance of secondary groove textures on the cell growth and adhesion. Grooves were textured with equivalent primary dimensions (Fig. 4.12a, d) but different secondary texture (Fig. 4.12b, e). Grooves cut with a final pass of higher energy yielded a greater roughness (Fig. 4.12b) and tended to have a much larger number of cells spanning multiple grooves (Fig. 4.12c) due to the presence of favorable attachment sites near the tops of the grooves. Other more complex patterns and interactions can be probed in this fashion.

Multiscale texturing of surfaces can have a profound impact on the growth and adhesion of cells on surfaces for such applications as structural implants or other medical devices. In these cases, it is not just the overall roughness or large scale morphology but also the detailed features on all length scales that affect the resulting material interaction. The unique laser-induced structures can modify the morphology and local chemistry of the surface making it more beneficial for cells to grow in certain patterns or to grow at a certain density depending on the features at various size scales. Using newer laser processing approaches opens the door to greater optimization in these important applications.

4.6 Conclusions

In this chapter, we have shown some of the versatile capabilities of laser processing to modify the surface properties of materials in order to enhance their performance for a variety of applications. The laser is a flexible tool that allows precise deposition of energy into the material at a controlled rate and within a confined area. A variety of different material responses can be achieved depending on the material system and the laser parameters, allowing processes to be designed and optimized to permanently alter the material's surface chemistry, crystal structure, and morphology to suite its desired function. The unique aspect of this for many applications is that the material modifications can occur over many different length scales, adding complexity to the surface and a new dimension to surface optimization. Laser surface processing has been a key element in a number of large-scale industrial manufacturing operations, yet at the same time it continues to reinvent itself and find ever new uses in emerging areas. As lasers continue to be developed with an ever broadening range of capabilities, laser surface processing will continue to improve the performance of materials in existing applications and will open the door to new materials and novel applications that would not be possible without these unique processing capabilities.

References

1. P. Campbell, J. Opt. Soc. Am. B **10**(12) (1993)
2. V. Semak, N. Dahotre, in *Lasers in Surface Engineering*, *Surface Engineering Series*, vol. 1, ed. by N. Dahotre (ASM International, Materials Park, OH, USA, 1998), pp. 35–67
3. M. Sheehy, B. Tull, C. Friend, E. Mazur, Mat. Sci. Eng. B **137**, 289 (2006)
4. V. Gregson, *Laser Material Processing* (Holland Publishing Company, Holland, 1984)
5. I. Etsion, J. Tribol. Trans. ASME **127**(1), 248 (2005)
6. N. Dahotre, *Lasers in Surface Engineering*, *Surface Engineering Series*, vol. 1 (ASM International, Materials Park, OH, USA, 1998)
7. D. Bäuerle, *Laser Processing and Chemistry* (Springer, Berlin, 2000)
8. W.M. Steen, *Laser Material Processing*, 3rd edn. (Springer, London, 2003)
9. J.C. Ion, *Laser Processing of Engineering Materials: Principles, Procedure and Industrial Applications* (Elsevier Butterworth-Heinemann, Oxford, 2005)
10. S.Y. Zhang, Y.H. Ren, G. Lupke, Appl. Opt. **42**(4), 715 (2003)
11. L.A. Romero, F.M. Dickey, J. Opt. Soc. Am. A: **13**(4), 751 (1996)
12. C. Momma, S. Nolte, G. Kamlage, F. von Alvensleben, A. Tunnermann, Appl. Phys. A Mater. Sci. Process. **67**(5), 517 (1998)
13. N. Sanner, N. Huot, E. Audouard, C. Larat, J.P. Huignard, B. Loiseaux, Opt. Lett. **30**(12), 1479 (2005)
14. K. Nemoto, T. Nayuki, T. Fujii, N. Goto, Y. Kanai, Appl. Opt. **36**(30), 7689 (1997)
15. E. McLeod, A.B. Hopkins, C.B. Arnold, Opt. Lett. **31**(21), 3155 (2006)
16. S. Heinemann, Opt. Commun. **119**(5–6), 613 (1995)
17. F.M. Dickey, S.C. Holswade (eds.), *Laser Beam Shaping: Theory and Techniques* (Marcel Dekker, New York, 2000)
18. E. Hecht, *Optics*, 4th edn. (Addison Wesley, San Francisco, 2002)
19. J. Heller, J.W. Bartha, C.C. Poon, A.C. Tam, Appl. Phys. Lett. **75**(1), 43 (1999)
20. M. Toulemonde, S. Unamuno, R. Heddache, M.O. Lampert, M. Hageali, P. Siffert, Appl. Phys. A Mater. Sci. Process. **36**(1), 31 (1985)
21. C.B. Arnold, M.J. Aziz, M. Schwarz, D.M. Herlach, Phys. Rev. B **59**(1), 334 (1999)
22. J.C. Weeber, J.R. Krenn, A. Dereux, B. Lamprecht, Y. Lacroute, J.P. Goudonnet, Phys. Rev. B **64**(4) (2001)
23. D.R. Lide, *CRC Handbook of Chemistry and Physics*, 82nd edn. (CRC, Boca Raton, 2001)
24. R.E. Slusher, B.J. Eggleton, *Nonlinear Photonic Crystals*, 1st edn. (Springer, Berlin, 2004)
25. N. Ghofraniha, C. Conti, G. Ruocco, S. Trillo, Phys. Rev. Lett. **99**(4) (2007)
26. W. Staudt, S. Borneis, K.D. Pippert, Phys. Status Solidi A Appl. Res. **166**(2), 743 (1998)
27. N. Mori, T. Ando, Phys. Rev. B **40**(9), 6175 (1989)
28. B.N. Chichkov, C. Momma, S. Nolte, F. vonAlvensleben, A. Tunnermann, Appl. Phys. A Mater. Sci. Process. **63**(2), 109 (1996)
29. M. von Allmen, A. Blatter, *Laser-Beam Interactions with Materials: Physical Principles and Applications*. Springer Series in Materials Science (Springer, Berlin, 1995)
30. Y. Hirayama, M. Obara, Appl. Surf. Sci. **197**, 741 (2002)
31. L.V. Zhigilei, P.B.S. Kodali, B.J. Garrison, J. Phys. Chem. B **101**(11), 2028 (1997)
32. A.J. Hick, Heat Treat. Met. **10**(1), 3 (1983)
33. D.L. Bourell, H.L. Marcus, J.W. Barlow, J.J. Beaman, Int. J. Powder Metall **28**(4), 369 (1992)
34. X. Wang, X. Xu, Appl. Phys. A Mater. Sci. Process. **73**(1), 107 (2001)
35. M.J. Aziz, J.Y. Tsao, M.O. Thompson, P.S. Peercy, C.W. White, Phys. Rev. Lett. **56**(23), 2489 (1986)
36. J.S. Im, M.A. Crowder, R.S. Sposili, J.P. Leonard, H.J. Kim, J.H. Yoon, V.V. Gupta, H.J. Song, H.S. Cho, Phys. Status Solidi A Appl. Res. **166**(2), 603 (1998)
37. T.D. Bennett, D.J. Krajnovich, C.P. Grigoropoulos, P. Baumgart, A.C. Tam, J. Heat Transfer **119**(3), 589 (1997)
38. S.C. Chen, D.G. Cahill, C.P. Grigoropoulos, J. Heat Transfer **122**(1), 107 (2000)
39. J. Eizenkop, I. Avrutsky, D.G. Georgiev, V. Chaudchary, J. Appl. Phys. **103**(9), 094311 (2008)

40. D.B. Chrisey, G.K. Hubler (eds.), *Pulsed Laser Deposition of Thin Films* (Wiley-Interscience, New York, 1994)
41. X.L. Mao, A.C. Ciocan, R.E. Russo, Appl. Spectrosc. **52**(7), 913 (1998)
42. N.M. Bulgakova, A.V. Bulgakov, Appl. Phys. A Mater. Sci. Process. **73**(2), 199 (2001)
43. R. Stoian, D. Ashkenasi, A. Rosenfeld, E.E.B. Campbell, Phys. Rev. B **62**(19), 13167 (2000)
44. B.J. Garrison, R. Srinivasan, J. Appl. Phys. **57**(8), 2909 (1985)
45. A.H. Clauer, B.P. Fairand, B.A. Wilcox, Metall. Mater. Trans. B **8**(12), 1871 (1977)
46. N.G. Semaltianos, W. Perrie, V. Vishnyakov, R. Murray, C.J. Williams, S.P. Edwardson, G. Dearden, P. French, M. Sharp, S. Logothetidis, K.G. Watkins, Mater. Lett. **62**(14), 2165 (2008)
47. J. Woodhead, J. Hergt, M. Shelley, S. Eggins, R. Kemp, Chem. Geol. **209**(1–2), 121 (2004)
48. X. Liu, D. Du, G. Mourou, IEEE J. Quantum Electron. **33**(10), 1706 (1997)
49. D.W. Zhang, T.C. Lei, J.G. Zhang, J.H. Ouyang, Surf. Coat. Technol. **115**(2–3), 176 (1999)
50. X.G. Wang, S.S. Li, C.H. Huang, S. Rawal, J.M. Howard, V. Craciun, T.J. Anderson, O.D. Crisalle, Sol. Energy Mater. Sol. Cells **88**(1), 65 (2005)
51. P. Baumgart, D.J. Krajnovich, T.A. Nguyen, A.C. Tam, IEEE Trans. Magn. **31**(6), 2946 (1995)
52. I. Etsion, Tribol. Lett. **17**(4), 733 (2004)
53. A.C. Tam, W.P. Leung, W. Zapka, W. Ziemlich, J. Appl. Phys. **71**(7), 3515 (1992)
54. R. Ranjan, D.N. Lambeth, M. Tromel, P. Goglia, Y. Li, J. Appl. Phys. **69**(8), 5745 (1991)
55. R. Blossey, Nat. Mater. **2**(5), 301 (2003)
56. V. Zorba, E. Stratakis, M. Barberoglou, E. Spanakis, P. Tzanetakis, C. Fotakis, Appl. Phys. A Mater. Sci. Process. **93**(4), 819 (2008)
57. M. Barberoglou, V. Zorba, E. Stratakis, E. Spanakis, P. Tzanetakis, S. Anastasiadis, C. Fotakis, Appl. Surf. Sci. **255**(10), 5425 (2009)
58. V. Zorba, P.D. Persano, L., A. Athanassiou, E. Stratakis, R. Cingolani, P. Tzanetakis, C. Fotakis, Nanotechnology **17**(13), 3234 (2006)
59. T.O. Yoon, H.J. Shin, S.C. Jeoung, Y.I. Park, Opt. Express **16**(17), 12715 (2008)
60. J. Wang, H. Chen, T. Sui, A. Li, D. Chen, Plant Science **176**(5), 687 (2009)
61. N.A. Patankar, Langmuir **20**(19), 8209 (2004)
62. D. Bouhafs, A. Moussi, A. Chikouche, J.M. Ruiz, Sol. Energy Mater. Sol. Cells **52**(1–2), 79 (1998)
63. W. Zhou, M. Tao, L. Chen, H. Yang, J. Appl. Phys. **102**(10) (2007)
64. O. Kluth, B. Rech, L. Houben, S. Wieder, G. Schope, C. Beneking, H. Wagner, A. Loffl, H.W. Schock, Thin Solid Films **351**(1–2), 247 (1999)
65. S.J. Wilson, M.C. Hutley, Opt. Acta **29**(7), 993–1009 (1982)
66. S.A. Boden, D.M. Bagnall, Appl. Phys. Lett. **93**(13), 133108 (2008)
67. J.H. Zhao, A.H. Wang, P. Campbell, M.A. Green, IEEE Trans. Electron Devices **46**(7), 1495 (1999)
68. H. Jansen, M. Deboer, R. Legtenberg, M. Elwenspoek, J. Micromech. Microeng. **5**(2), 115 (1995)
69. H. Nakaya, M. Nishida, Y. Takeda, S. Moriuchi, T. Tonegawa, T. Machida, T. Nunoi, Sol. Energy Mater. Sol. Cells **34**(1–4), 219 (1994)
70. J.C. Zolper, S. Narayanan, S.R. Wenham, M.A. Green, Appl. Phys. Lett. **55**(22), 2363 (1989)
71. M. Abbott, J. Cotter, Prog. Photovoltaics Res. Appl. **14**(3), 225 (2006)
72. L. Dobrzański, A. Drygała, K. Gołombek, P. Panek, E. Bielańska, P. Zięba, J. Mater. Process. Technol. **201**(1–3), 291 (2008)
73. M. Halbwax, T. Sarnet, P. Delaporte, M. Sentis, H. Etienne, F. Torregrosa, V. Vervisch, I. Perichaud, S. Martinuzzi, Thin Solid Films **516**(20), 6791 (2008)
74. M. Birnbaum, J. Appl. Phys. **36**(11), 3688 (1965)
75. H.M. van Driel, J.E. Sipe, J.F. Young, Phys. Rev. Lett. **49**(26) (1982)
76. Z. Guosheng, P.M. Fauchet, A.E. Siegman, Phys. Rev. B **26**, 5366 (1982)
77. J.E. Sipe, J.F. Young, J.S. Preston, H.M. van Driel, Phys. Rev. B **27**, 1141 (1983)
78. E.M. Hsu, T.H.R. Crawford, C. Maunders, G.A. Botton, H.K. Haugen, Appl. Phys. Lett. **92**(22) (2008)
79. D. Dufft, A. Rosenfeld, S.K. Das, R. Grunwald, J. Bonse, J. Appl. Phys. **105**(3) (2009)

80. A.Y. Vorobyev, G. Chunlei, J. Appl. Phys. **103**(4), 043513 (2008)
81. S.R. Foltyn, *Pulsed Laser Deposition of Thin Films* (Wiley-Interscience, New York, 1994)
82. F. Sánchez, J.L. Morenza, R. Aguiar, J.C. Delgado, M. Varela, Appl. Phys. Lett. **69**(5) (1996)
83. Y. Kawakami, E. Ozawa, Appl. Surf. Sci. **218**(1–4), 175 (2003)
84. A. Bensaoula, C. Boney, R. Pillai, G.A. Shafeev, A.V. Simakin, D. Starikov, Appl. Phys. A Mater. Sci. Process. **79**(4–6), 973 (2004)
85. Y. Yang, J.J. Yang, C.Y. Liang, H.S. Wang, Opt. Express **16**(15), 11259 (2008)
86. A.Y. Vorobyev, C. Guo, J. Appl. Phys. **104**(5) (2008)
87. D.H. Lowndes, J.D. Fowlkes, A.J. Pedraza, Appl. Surf. Sci. **154–155**, 647 (2000)
88. V.V. Voronov, S.I. Dolgaev, S.V. Lavrishchev, A.A. Lyalin, A.V. Simakin, G.A. Shafeev, Quantum Electron. **30**, 710 (2000)
89. A.J. Pedraza, J.D. Fowlkes, S. Jesse, C. Mao, D.H. Lowndes, Appl. Surf. Sci. **168**(1–4), 251 (2000)
90. S. Dolgaev, S. Lavrishev, A. Lyalin, A. Simakin, V. Voronov, G. Shafeev, Appl. Phys. A **73**(2), 177 (2001)
91. J. Bonse, S. Baudach, J. Krüger, W. Kautek, M. Lenzner, Appl. Phys. A **74**(1) (2002)
92. B.R. Tull, J.E. Carey, E. Mazur, J.P. McDonald, S.M. Yalisove, MRS Bull. **31**(8), 626 (2006)
93. X.Y. Chen, J. Lin, J.M. Liu, Z.G. Liu, Appl. Phys. A (2008)
94. T.H. Her, R.J. Finlay, C. Wu, S. Deliwala, E. Mazur, Appl. Phys. Lett. **73**(12) (1998)
95. M.A. Sheehy, L. Winston, J.E. Carey, C.M. Friend, E. Mazur, Chem. Mater. **17**, 3582 (2005)
96. M. Shen, C.H. Crouch, J.E. Carey, E. Mazur, Appl. Phys. Lett. **85**, 5694 (2004)
97. C.H. Crouch, J.E. Carey, J.M. Warrender, M.J. Aziz, E. Mazur, F.Y. Génin, Appl. Phys. Lett. **84**, 1850 (2004)
98. C. Wu, C.H. Crouch, L. Zhao, J.E. Carey, R. Younkin, J.A. Levinson, E. Mazur, R.M. Farrell, P. Gothoskar, A. Kager, Appl. Phys. Lett. **78**(1850) (2001)
99. J.E. Carey, C.H. Crouch, M. Shen, E. Mazur, Opt. Lett. **30**, 1773 (2005)
100. Z. Huang, J.E. Carey, M. Liu, X. Guo, E. Mazur, J.C. Campbell, Appl. Phys. Lett. **89** (2006)
101. R.A. Myers, R. Farrell, A.M. Karger, J.E. Carey, E. Mazur, Appl. Opt. **45**, 8825 (2006)
102. B. Ratner, A. Hoffman, F. Schoen, J. Lemons, *Biomaterials Science: An Introduction to Materials in Medicine* Second Edition (Elsevier Acedemic Press, Sand Diego, CA, 2004)
103. D. Brunette, *Titanium in Medicine: Material Science, Surface Science, Engineering, Biological Responses, and Medical Applications* (Springer, New York, 2001)
104. S.K. Gupta, A. Chu, A.S. Ranawat, J. Slamin, C.S. Ranawat, J. Arthroplast. **22**(6), 787 (2007)
105. B. Kasemo, J. Lausmaa, CRC Critical Reviews in Biocompatibility **2**(4), 335 (1986)
106. D.A. Puleo, A. Nanci, Biomaterials **20**(23–24), 2311 (1999)
107. K. Anselme, Biomaterials **21**(7), 667 (2000)
108. U. Meyer, A. Büchter, H. Wiesmann, U. Joos, D. Jones, European Cells and Materials **9**, 39 (2005)
109. M. Wong, J. Eulenberger, R. Schenk, E. Hunziker, J. Biomed. Mater. Res. **29**(12), 1567 (1995)
110. J. Park, J. Bronzino, Y. Kim, *Biomaterials: Principles and Applications* (CRC Press, Boca Raton, USA, 2003)
111. A. Curtis, C. Wilkinson, Biomaterials **18**(24), 1573 (1997)
112. J. Tan, W.M. Saltzman, Biomaterials **25**(17), 3593 (2004)
113. T.G. Vankooten, J.M. Schakenraad, H.C. Vandermei, H.J. Busscher, Biomaterials **13**(13), 897 (1992)
114. D.M. Brunette, Int. J. Oral Maxillofac. Implants **3**(4), 231 (1988)
115. R.G. Flemming, C.J. Murphy, G.A. Abrams, S.L. Goodman, P.F. Nealey, Biomaterials **20**(6), 573 (1999)
116. A. Khakbaznejad, B. Chehroudi, D.M. Brunette, J. Biomed. Mat. Res. A **70A**(2), 206 (2004)
117. W.O. Soboyejo, B. Nemetski, S. Allameh, N. Marcantonio, C. Mercer, J. Ricci, J. Biomed. Mater. Res., Part A **62**(1), 56 (2002)
118. M.D. Ward, D.A. Hammer, Biophys. J. **64**, 936 (1993)
119. N. Wang, J.P. Butler, D.E. Ingber, Science **260**(5111), 1124 (1993)
120. E.T. den Braber, J.E. de Ruijter, H.T.J. Smits, L.A. Ginsel, A.F. von Recum, J.A. Jansen, Biomaterials **17**(11), 1093 (1996)

121. E.T. den Braber, J.E. de Ruijter, L.A. Ginsel, A.F. von Recum, J.A. Jansen, J. Biomed. Mater. Res. **40**(2), 291 (1998)
122. A. Kurella, N.B. Dahotre, J. Biomater. Appl. **20**(1), 5 (2005)
123. J. Lawrence, L. Hao, H.R. Chew, Surf. Coat. Technol. **200**(18–19), 5581 (2006)
124. R. Singh, S.G. Chowdhury, S.K. Tiwari, N.B. Dahotre, J. Mater. Sci. Mater. Med. **19**(3), 1363 (2008)
125. D.L. Cochran, D. Buser, C.M. ten Bruggenkate, D. Weingart, T.M. Taylor, J.P. Bernard, F. Peters, J.P. Simpson, Clin. Oral Implants Res. **13**(2), 144 (2002)
126. J.H.C. Wang, E.S. Grood, J. Florer, R. Wenstrup, J. Biomech. **33**(6), 729 (2000)
127. K. Anselme, B. Noel, P. Hardouin, J. Mater. Sci. Mater. Med. **10**(12), 815 (1999)
128. C. Hallgren, H. Reimers, D. Chakarov, J. Gold, A. Wennerberg, Biomaterials **24**(5), 701 (2003)
129. J.P. Ulerich, L.C. Ionescu, J. Chen, W.O. Soboyejo, C.B. Arnold, in *Photon Processing in Microelectronics and Photonics VI*, ed. by C.B. Arnold, T. Okada, M. Meunier, A.S. Holmes, D.B. Geohegan, F. Träger, J.J. Dubowski (San Jose, 2007)
130. A.Y. Fasasi, S. Mwenifumbo, N. Rahbar, J. Chen, M. Li, A.C. Beye, C.B. Arnold, W.O. Soboyejo, Mater. Sci. Eng. C **29**(1), 5 (2009)
131. J. Chen, J. Ulerich, E. Abelev, A. Fasasi, C.B. Arnold, W.O. Soboyejo, Mater. Sci. Eng. C **29**(4), 1442 (2009)